ACS APPLIED MATERIALS & INTERFACES

Research Article

www.acsami.org

Integrin $\alpha_V\beta_3$-Targeted Magnetic Nanohybrids with Enhanced Antitumor Efficacy, Cell Cycle Arrest Ability, and Encouraging Anti-Cell-Migration Activity

Guo-Bin Ding,[†,‡] Yan Wang,[†] Yi Guo,*[,†] and Li Xu*[,†,§]

[†]Key Laboratory for Molecular Enzymology and Engineering, the Ministry of Education, College of Life Science, and [§]National Engineering Laboratory for AIDS Vaccine, Jilin University, Changchun 130012, People's Republic of China

[‡]Institute of Biotechnology, the Key Laboratory of Chemical Biology and Molecular Engineering of Ministry of Education, Shanxi University, Taiyuan 030006, People's Republic of China

Supporting Information

ABSTRACT: Organic/inorganic nanohybrids, which integrate advantages of the biocompatibility of organic polymers and diversified functionalities of inorganic nanoparticles, have been extensively investigated in recent years. Herein, we report the construction of arginine-glycine-aspartic acid-cysteine (RGDC) tetrapeptide functionalized and 10-hydroxycamptothecin (HCPT)-encapsulated magnetic nanohybrids (RFHEMNs) for integrin $\alpha_V\beta_3$-targeted drug delivery. The obtained RFHEMNs were near-spherical in shape with a homogeneous size about 50 nm, and exhibited a superparamagnetic behavior. In vitro drug release study showed a sustained and pH-dependent release profile. Cell viability tests revealed that RFHEMNs displayed a significant enhancement of cytotoxicity against $\alpha_V\beta_3$-overexpressing A549 cells, as compared to free HCPT and nontargeting micelles. Flow cytometry analysis indicated that this cytotoxic effect was associated with dose-dependent S phase arrest. Finally, RFHEMNs exerted encouraging anti-cell-migration activity as determined by an in vitro wound-healing assay and a transwell assay. Overall, we envision that this tumor-targeting nanoscale drug delivery system may be of great application potential in chemotherapy of primary tumor and their metastases.

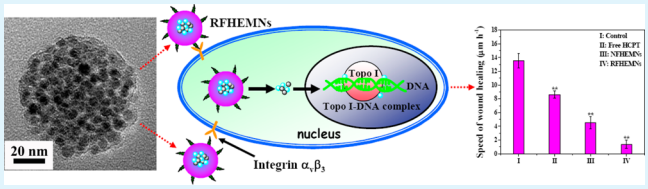

KEYWORDS: *RGDC tetrapeptide, integrin targeting, magnetic nanohybrids, antitumor efficacy, cell cycle, anti-cell-migration*

1. INTRODUCTION

Amphiphilic copolymers can spontaneously self-assemble into core−shell structure polymeric micelles with a diameter of 10−200 nm under appropriate conditions.[1−3] These polymer micelles have been extensively employed in numerous biomedical applications, particularly in targeted drug delivery,[4,5] because of high stability, chemical flexibility, satisfying drug loading content, increased cellular uptake of the loaded drugs, and preferential accumulation in solid tumors via the passive "enhanced permeability and retention (EPR) effect".[6,7] Comparatively, the inorganic magnetic iron oxide nanoparticles (NPs) have been arousing increasing interest not only for their ease of synthesis, small size, good biocompatibility, and unique superparamgnetism,[8] but also for their potential applications in biomedical fields,[9,10] such as protein purification,[11] enzyme immobilization,[12] removal of metal ions,[13] toxin detection,[14] drug/gene delivery,[15] and enhancement of contrast in magnetic resonance imaging (MRI)[16] etc. The combination of organic polymers and inorganic magnetic NPs can completely perform advantage of each and produce magnetic nanohybrids with some desirable properties.[17−19]

10-Hydroxycamptothecin (HCPT), a natural analogue of camptothecin (CPT), has a strong antitumor activity against a broad spectrum of solid tumors, such as gastric carcinoma, ovarian cancer, hepatoma, breast cancer, bladder carcinoma, leukemia, lung cancer, and tumor of head and neck in clinical trials.[20,21] Moreover, it has been demonstrated that HCPT is more active and less toxic compared with CPT.[22] However, the poor solubility and labile lactone ring of HCPT greatly restrict its therapeutic potential.[23−25] With the emergence and remarkable development of nanobiotechnology in recent years, much research effort has been directed to the design and synthesis of high performance nanoscale HCPT delivery systems such as lipid-polymer composite,[26] dendrimers,[27] nanoparticles,[28] and polymer micelles,[20,22] so that the stability and solubility problems could be overcome. Very recently, magnetic nanohybrids have also been used for HCPT delivery by using Fe_3O_4 nanoparticles as cores and PEG conjugated chitosan (PEG-CS) as a polymeric shell, and the cytotoxicity increased significantly in comparison with free HCPT.[29]

All the aforementioned nanoscale HCPT delivery systems focused on inhibiting the tumor cells' ability to proliferate. However, one of the major obstacles for successful cancer therapy is tumor metastasis,[30] and more than 90% of the cancer

Received: May 30, 2014
Accepted: September 10, 2014
Published: September 10, 2014

mortality is due to the metastatic property of cancer.[31] Cell migration plays a critical role in the process of tumor metastasis.[32] Therefore, metastasis is a potential therapeutic target for malignant tumor, and block or suppress the migratory capacity of tumor cells provides a new strategy for achieving better survival from cancer.[33] Unfortunately, despite its significance, study on the antimetastatic activity of drug-loaded nanocarriers has so far received little attention. In our previous study, an HCPT-encapsulated magnetic nanovehicle (HEMN) has been developed by incorporating HCPT into the magnetic nanohybrids, and the HEMNs could be effectively internalized into cells at targeted sites under external magnetic guidance to selectively kill cells in that area.[22] Nevertheless, the magnetic nanovehicles did not have the active targeting ability. The passive targeting based on the EPR effect has some limitations because large tumors exhibit great pathophysiological heterogeneity.[34] The extent of tumor permeability (cutoff pore size) varied depending on the tumor type,[35,36] and some parts of tumors do not display the EPR effect.[34] Thus, it is indispensible to develop more efficacious HCPT-delivery systems with active targeting ability and investigate their antimetastatic activity.

As an important member of integrin family, the adhesion molecule $\alpha_V\beta_3$ has been widely investigated for tumor imaging and therapy owing to its pivotal roles in tumor angiogenesis and metastasis.[37] In particular, due to its upregulated expression on tumor vasculature and proliferating tumor endothelial cells compared to resting endothelial cells and most normal tissues with low $\alpha_V\beta_3$ expression, integrin $\alpha_V\beta_3$ has been identified as an ideal therapeutic target for tumor chemotherapy.[38] The peptide ligands containing the RGD (arginine-glycine-aspartic acid) motif, which shows a strong binding affinity and selectivity to integrin $\alpha_V\beta_3$, have been employed as tumor-homing ligand to conjugate with various nanomedicine for integtrin targeted therapeutic applications.[37]

Herein, we report an organic/inorganic hybrid nanoplatform with active targeting ability, which is constructed by embedding Fe_3O_4 NPs and HCPT into polymer micelles, and then coupling cancer-targeting moiety RGDC to their surface. The targeting effect of RGDC functionalized and 10-hydroxycamptothecin-encapsulated magnetic nanohybrids (RFHEMNs) on the cell proliferation, cell cycle progression, and cell migration of A549 cells was investigated.

2. EXPERIMENTAL SECTION

2.1. Materials. D,L-Lactide (≥99.5 mol %) and glycolide (≥99.5 mol %) were purchased from Beijing GLACO Ltd. Maleimide-poly(ethylene glycol) (Mal-PEG-OH, M_n = 5 kDa) was obtained from JenKem technology Co. Ltd. (Beijing, China). Monomethoxy-polyethylene glycol (MPEG-OH, M_n = 5 kDa), stannous octoate [$Sn(Oct)_2$], and 3-(4,5-dimethylthiazol-2-yl)-2,5-diphenyltetrazolium bromide (MTT) were purchased from Sigma-Aldrich. 10-Hydroxycamptothecin (HCPT, ≥99%) was obtained from Chengdu Lanbei Plant Chemical Science and Technology Co. Ltd. (China). Tetrapeptide RGDC was purchased from Shanghai GL Biochem (China). Propidium iodide (PI) and RNase were obtained from Beijing Solarbio Science & Technology Co., Ltd. and Beyotime Institute of Biotechnology (China), respectively. Magnetite nanoparticles were synthesized according to our previous report.[39] All organic solvents used were of analytical grade. High-purity Milli-Q water with a resistivity of 18.2 MΩ cm was used in all the experiments.

2.2. Characterization. Gel permeation chromatography (GPC) measurements were carried out on a Waters 410 GPC with tetrahydrofuran (THF) as eluent (flow rate: 1.0 mL/min). The molecular weights were calibrated with polystyrene (PS) standards. ^{1}H NMR analysis was performed on Bruker Avance 500 MHz spectrometer at room temperature with tetramethylsilane (TMS) as the internal reference, using deuterated chloroform ($CDCl_3$) or DMSO-d6 as the solvent. TEM analysis was conducted on a JEOL JEM-1200EX model transmission electron microscope using an operating voltage of 100 kV. For negative staining, the sample was dropped onto a carbon-coated copper grid, stained with 2 wt % sodium phosphotungstate aqueous solution, and imaged within 24 h of staining. The hydrodynamic diameters of RGDC-functionalized and HCPT-encapsulated magnetic nanohybrids (RFHEMNs) were determined using a Brookhaven ZetaPALS dynamic light scattering (DLS) instrument with a BI-90Plus digital autocorrelator at a wavelength of 656 nm at 25 °C. The magnetic properties of RFHEMNs were studied using a physical property measurement system (PPMS, Quantum Design) at 10, 300, and 310 K.

2.3. Synthesis of MPEG-PLGA and Mal-PEG-PLGA Copolymers. These two copolymers were prepared by ring-opening polymerization of D,L-Lactide (≥99.5 mol %) and glycolide in the presence of MPEG−OH or Mal-PEG-OH, and stannous octoate was used as catalyst. In brief, in a three-neck round-bottom flask, MPEG-OH or Mal-PEG-OH (0.1 g), D,L-lactide (0.25 g), glycolide (0.05 g), and stannous octoate (3 mg) were introduced to freshly distilled toluene, heated to reflux with magnetic stirring under a nitrogen atmosphere for 9 h and then cooled to room temperature. The reaction mixture was processed essentially as previously described,[39] and the polymer product was obtained via lyophilization and stored under −20 °C before use.

2.4. Fabrication of RGDC Functionalized and 10-Hydroxycamptothecin-Encapsulated Magnetic Nanohybrids (RFHEMNs). Mal-PEG-PLGA copolymer (10 mg), HCPT (2 mg), and magnetite NPs (2 mg) were dissolved in a mixed solvent of tetrahydrofuran (THF) and DMSO (2 mL, 1:1). The mixture was added dropwise to water under sonication, then RGDC (0.5 mg) was added and stirred. The Michael addition reaction was allowed to occur for 4 h followed by dialyzation against water for 48 h to allow the formation of micelles and to remove organic solvents, free RGDC and unencapsulated HCPT (M_w cutoff: 12 000−14 000 Da). Finally, the micelle solution was filtered through a filter to eliminate HCPT and magnetite aggregates. The nonfunctionalized and 10-hydroxycamptothecin-encapsulated magnetic nanohybrids (NFHEMNs) were prepared by a similar method using MPEG-PLGA copolymer.

2.5. In Vitro Release of HCPT from RFHEMNs. The release profiles of HCPT from RFHEMNs in vitro were studied by a dialysis method in PBS (pH 7.4) and 0.1 M sodium acetate buffer (pH 5.0) at 37 °C.[22] RFHEMNs micellar solution was placed in a dialysis bag (M_w cutoff: 12 000−14 000 Da) and immersed into the release medium (80 mL) with gentle agitation. At predetermined time intervals, the micellar solution in the dialysis bag was withdrawn, dissolved in DMSO, centrifuged (12 000 rpm, 30 min) to remove magnetite NPs and subjected to UV/vis analysis to determine the residual HCPT content. Finally, the amount of drug released was calculated.

2.6. In Vitro Cytotoxicity. Cytotoxicity against A549 (human nonsmall cell lung carcinoma cells) and HEK293T (human embryonic kidney cells 293T) cells was evaluated by standard MTT cell viability assay. Cells were seeded in 96-well plates at a density of 5×10^3 cells per well and incubated in Dulbecco's modified Eagle's medium (DMEM; Gibco) containing 10% fetal bovine serum (FBS) at 37 °C and under 5% CO_2 for 24 h. The culture medium was replaced by free HCPT, NFHEMNs or RFHEMNs with increasing concentrations of HCPT (from 0.01−100 μM). After treatment for 24 h, 20 μL of MTT solution (5 mg/mL in PBS) was added and further incubated for 4 h. The formazan precipitate was then dissolved in DMSO (150 μL) and cell viabilities were analyzed and recorded on a microplate reader (Biorad, USA).

2.7. Analysis of Cell Cycle Distribution by Fow Cytometry. A549 cells (5×10^5 cells per well) were seeded in 6-well plates, incubated for 24 h, and treated with free HCPT, NFHEMNs or RFHEMNs with different concentrations of HCPT (0.01, 0.1, and 1 μM) for 12 h. Then the cells were harvested with trypsin, washed with PBS, and fixed by cold 70% ethanol. Subsequently, cells were treated

with RNase A, labeled with propidium iodide, and analyzed by a flow cytometer (Becton Dickinson, San Jose, CA).

2.8. Anti-Cell-Migration Study. *In Vitro Wound-Healing Assay.* To assess cell motility, A549 cells (5×10^5 cells per well) were seeded in 24-well plates and cultured as confluent monolayers. The monolayers were scraped with a sterile white micropipette tip (0 h) to create a denuded zone with constant width and washed twice to remove cellular debris. The cells were exposed to free HCPT, NFHEMNs or RFHEMNs (with an HCPT concentration of 100 μM) for 6 h. The medium was then replaced with fresh DMEM containing 2% FBS. At 0 and 24 h, the scratched monolayers were photographed by using an inverted microscope (Olympus) and the scratch width was determined. Wound healing was quantified as the average linear speed of the wound edges over 24 h.

Transwell Migration Assays. A549 cells were seeded into the upper chamber of a transwell insert (6.5 mm diameter, 8 mm pores; Corning, New York, USA) at a density of 1.5×10^4 cells per well, DMEM (500 mL) with 10% FBS was added to the lower chamber, and the 24-well plate was incubated for 24 h. The cells were treated with free HCPT, NFHEMNs or RFHEMNs (with an HCPT concentration of 100 μM) for 6 h. The medium in the top chamber was then replaced with serum-free DMEM medium and the medium in the lower chamber was replaced with fresh DMEM containing 10% FBS. Cells were incubated for 24 h, and the nonmigrated cells were scraped off the upper surface of the membrane with a cotton swab. MTT assay was used to determine the migrated cells remaining on the bottom surface. The migration rate (percentage of migrated cells) was calculated according to eq 1, in which OD_{mig} is the optical density (OD) of migrated cells and OD_{total} is the OD of total cells. The degree of inhibition of cell migration was calculated according to eq 2, in which Mig_{ctrl} and Mig_t are the migration rate of control and treated cells, respectively.

$$\text{migration rate}\ (\%) = OD_{mig}/OD_{total} \times 100\% \quad (1)$$

$$\text{inhibition of migration}\ (\%) = (Mig_{ctrl} - Mig_t)/Mig_{ctrl} \times 100\% \quad (2)$$

2.9. Statistical Analysis. All data are presented as the mean ± SD (standard deviations). Statistical significance between the control and test groups was evaluated by Student's *t* test. The differences were considered statistically significant when $P < 0.05$.

3. RESULTS AND DISCUSSION

3.1. Characterization of MPEG-PLGA and Mal-PEG-PLGA Copolymers. First, gel permeation chromatography (GPC) was used to determine the molecular weight and its distribution (polydispersity index, PDI) of these two copolymers. As listed in Table 1, MPEG-PLGA has a number-average molecular weight (Mn) of 11626 Da and a PDI of 1.360, whereas the M_n and PDI of Mal-PEG-PLGA copolymer were 10034 Da and 1.295, respectively. Thus, the obtained copolymers have a similar Mn and a relatively narrow molecular weight distribution. Then, the molecular structure of the copolymers was verified by ^{1}H NMR spectroscopy and the spectra are shown in Figure 1, in which all the peaks from the copolymers are assigned to specific chemical groups. There are some common peaks for the two copolymers, including the sharp peak at 3.64 ppm (methylene groups of the PEG), the peaks at 1.57 and 5.19 ppm (methyl group and the −CH− group of D,L-lactide repeat units) and the peaks around 4.82 ppm (the $-CH_2-$ group of the glycolide repeat units). The small peak appeared at 3.38 ppm corresponds to $-OCH_3$ groups of the MPEG unit in MPEG-PLGA copolymer (Figure 1a), while the characteristic resonance detected at around 6.70 ppm is assigned to the maleimide groups of Mal-PEG-PLGA copolymer (the inset in Figure 1b). These results testify to the successful synthesis of these two copolymers. The Mn of MPEG-PLGA and Mal-PEG-PLGA copolymers calculated from the ^{1}H NMR spectra were 15486 and 14880 Da, respectively (Table 1). This difference of Mn between NMR calculation and GPC measurements is also reported by Ding's group and may arise from different standards.[40]

Table 1. MPEG-PLGA and Mal-PEG-PLGA Copolymer Used in This Study

sample	M_n[a] (Da)	PDI[a]	M_n[b] (Da)
MPEG-PLGA	11626	1.360	15486
Mal-PEG-PLGA	10034	1.295	14880

[a]determined by GPC. [b]calculated from ^{1}H NMR.

3.2. Preparation and Characterization of RGDC Functionalized and 10-Hydroxycamptothecin-Encapsulated Magnetic Nanohybrids (RFHEMNs). To validate that the Michael addition reaction occurs between the sulfhydryl group of RGDC and the maleimide of Mal-PEG-PLGA copolymer, we used Mal-PEG-PLGA copolymers to prepare empty micelles by a dialysis method and RGDC was coupled to the micelle surface, obtaining the RGDC-functionalized PEG-PLGA (RGDC-PEG-PLGA) empty micelles. The ^{1}H NMR spectra of tetrapeptide RGDC and RGDC-PEG-PLGA empty micelles were presented in Figure 2. All the signals from the RGDC are ascribed to specific functional groups (Figure 2a). The successful conjugation of RGDC with Mal-PEG-PLGA copolymer was proven by the peaks from peptide bonds (−NH−CO−) of RGDC appeared at around 8.23 ppm (Figure 2b, inset (i)) and the absence of maleimide signal at around 6.70 ppm (Figure 2b, inset (ii)) when compared to Figure 1b.

As shown schematically in Scheme 1, RGDC-functionalized and 10-hydroxycamptothecin-encapsulated magnetic nanohybrids (RFHEMNs) were prepared by simultaneously incorporating magnetite nanoparticles and HCPT into the polymeric micelles self-assembled from Mal-PEG-PLGA amphiphilic copolymer through a facile dialysis method, and then conjugating RGDC to the surface of these micelles via a maleimide-mediated covalent binding procedure. A reasonable drug loading content of (6.63 ± 0.16)% was achieved in RFHEMNs, thus the water solubility of HCPT was largely improved. The drug loading content of RFHEMNs is a little lower than a recently developed magnetic polymer-based nanohybrid,[29] this is probably due to the different preparation methods. RFHEMNs were fabricated by two steps (drug loading and RGDC conjugation) and some loaded HCPT could release from the micelles during the RGDC coupling process, whereas the HCPT-loaded magnetic nanohybrids in ref 29 were prepared by a one-step precipitation method. For comparison, RGDC-functionalized empty micelles (RFEMs) were also fabricated.

Particle size of drug delivery systems is of key importance for the cellular uptake and plays a critical role in EPR effect of tumor tissues.[41] Transmission electron microscopy (TEM) images provide direct evidence for the formation of polymer micelles with a distinct core−shell structure and indicate that RFEMs and RFHEMNs have a well-defined spherical shape with an average particle size of about 20 and 50 nm, respectively (Figure 3a, b). It is apparent that a cluster of magnetite nanoparticles have been embedded in the hydrophobic cores (Figure 3b). Compared to RFEMs, the increase in size of RFHEMNs indicated the successful loading of magnetite nanoparticles and HCPT. DLS was used to characterize the

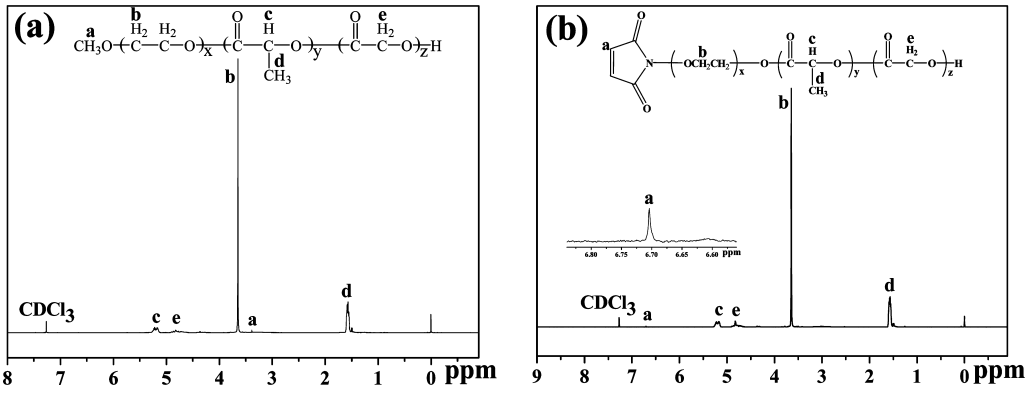

Figure 1. ^{1}H NMR spectra of (a) MPEG-PLGA and (b) Mal-PEG-PLGA copolymer in $CDCl_3$. The inset in (b) represents magnification of 6.5−6.9 ppm, in which the maleimide signal can be clealy seen at 6.70 ppm.

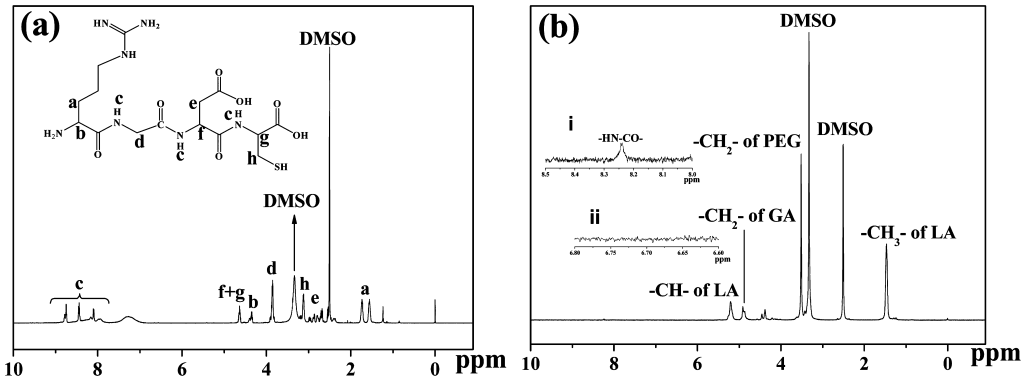

Figure 2. ^{1}H NMR spectra of (a) tetrapeptide RGDC and (b) RGDC-PEG-PLGA empty micelles in DMSO-d6. The insets i and ii in b represent magnification of 8.0−8.5 and 6.6−6.8 ppm, respectively, in which the peptide bond signal from RGDC can be seen at 8.23 ppm, whereas the maleimide signal at 6.70 ppm can not be detected.

Scheme 1. Schematic Diagrams Illustrating the Preparation of RGDC Functionalized and 10-Hydroxycamptothecin-Encapsulated Magnetic Nanohybrids (RFHEMNs) via a Dialysis Method and Their Interaction with Integrin $\alpha_V\beta_3$-Overexpressing Cells

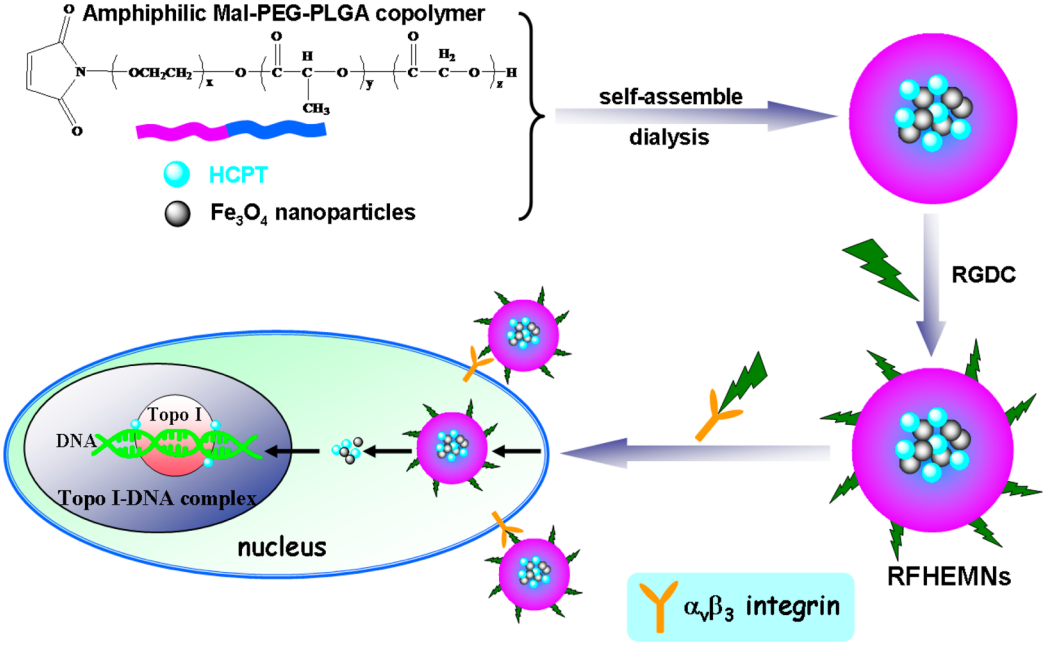

hydrodynamic size and its distribution of RFEMs and RFHEMNs, and the results were displayed in the insets of Figure 3a, b. The mean hydrodynamic diameter of RFEMs and RFHEMNs were 144 and 197 nm, respectively. An increase in

dx.doi.org/10.1021/am503359g | ACS Appl. Mater. Interfaces 2014, 6, 16643−16652

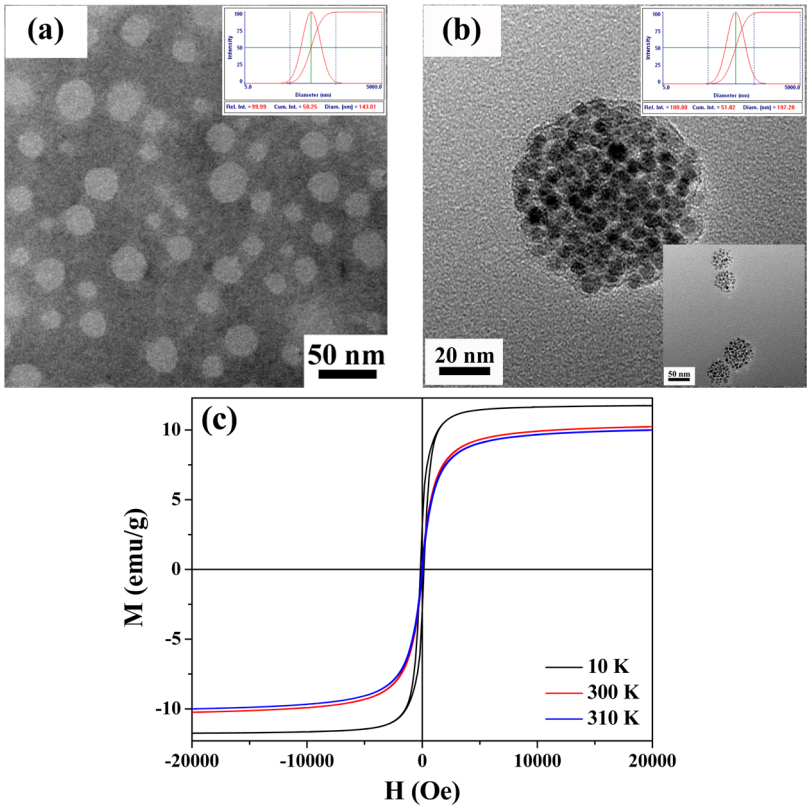

Figure 3. (a) TEM images of RGDC-functionalized empty micelles (RFEMs) after negative staining with 2% sodium phosphotungstate, the insets represent the hydrodynamic size and size distributions determined by DLS; (b) TEM images of RFHEMNs, the upper-right and lower-right insets shows hydrodynamic size distribution and TEM images of RFHEMNs at low magnification, respectively; (c) magnetization curve for the RFHEMNs at 10, 300, and 310 K.

the size of RFHEMNs was also observed, which is consistent with the TEM results. The polydispersity of RFEMs and RFHEMNs were 0.220 and 0.216, respectively, suggesting a relatively narrow size distribution. The great disparity in size determined by TEM and DLS may be attributed to the difference of two measuring techniques. The larger hydrodynamic diameter obtained from DLS relative to TEM was probably due to the existence of a PEG hydration layer around the core.[42] The SEM image of RFHEMNs also provided evidence that they had a spherical shape and showed homogeneous size distribution with diameter of about 50 nm (see the Supporting Information, Figure S1).

The magnetic property of the RFHEMNs was investigated by PPMS at 10K, 300 and 310 K with the magnetic field range 0−20 kOe. It can be seen from Figure 3c that RFHEMNs displayed ferromagnetic characteristics at 10 K with a coercivity of 136 Oe and a saturation magnetization of 11.75 emu/g. By comparison, no detectable coercivity and magnetic remanence is observed at 300 and 310 K, thus RFHEMNs exhibit typical superparamagnetic behavior at room and body temperature, with the saturation magnetization about 10.25 and 10.01 emu/g, respectively, which is sufficient for magnetic field guided drug delivery.[8,22]

3.3. Drug Release Study. To understand the release behavior of HCPT from RFHEMNs, in vitro release studies were performed in two most commonly used conditions—a simulated physiological solution (PBS, pH 7.4) and an acidic environment (sodium acetate buffer, pH 5.0). The relationship of the amount of HCPT released from RFHEMNs with time is shown in Figure 4. It was observed that the release profiles of HCPT from RFHEMNs in both solutions exhibit the characteristic of sustained release.

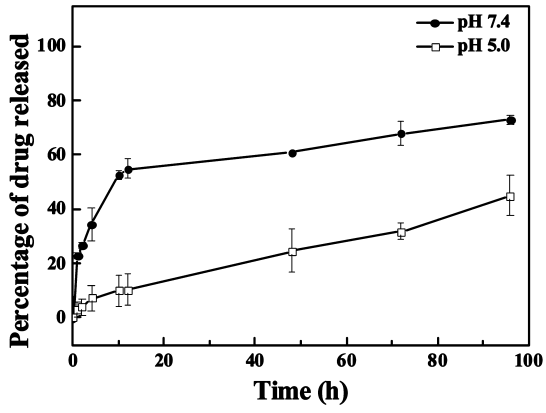

Figure 4. In vitro release profiles of HCPT from RFHEMNs under neutral (pH 7.4) and acidic conditions (pH 5.0) at 37 °C. The results are expressed as mean ± standard deviation (SD) from three independent experiments.

It is worth stressing that HCPT release profiles are pH-dependent. At physiological pH 7.4, the drug release was considerably faster compared with mildly acidic pH 5.0. The amount of HCPT release reached about 70% at pH 7.4 after 96 h. However, only about 45% release was observed in the same amount of time at pH 5.0, which indicates a good stability of RFHEMNs under acidic conditions. This remarkable difference can be explained by the instability of HCPT at higher pH

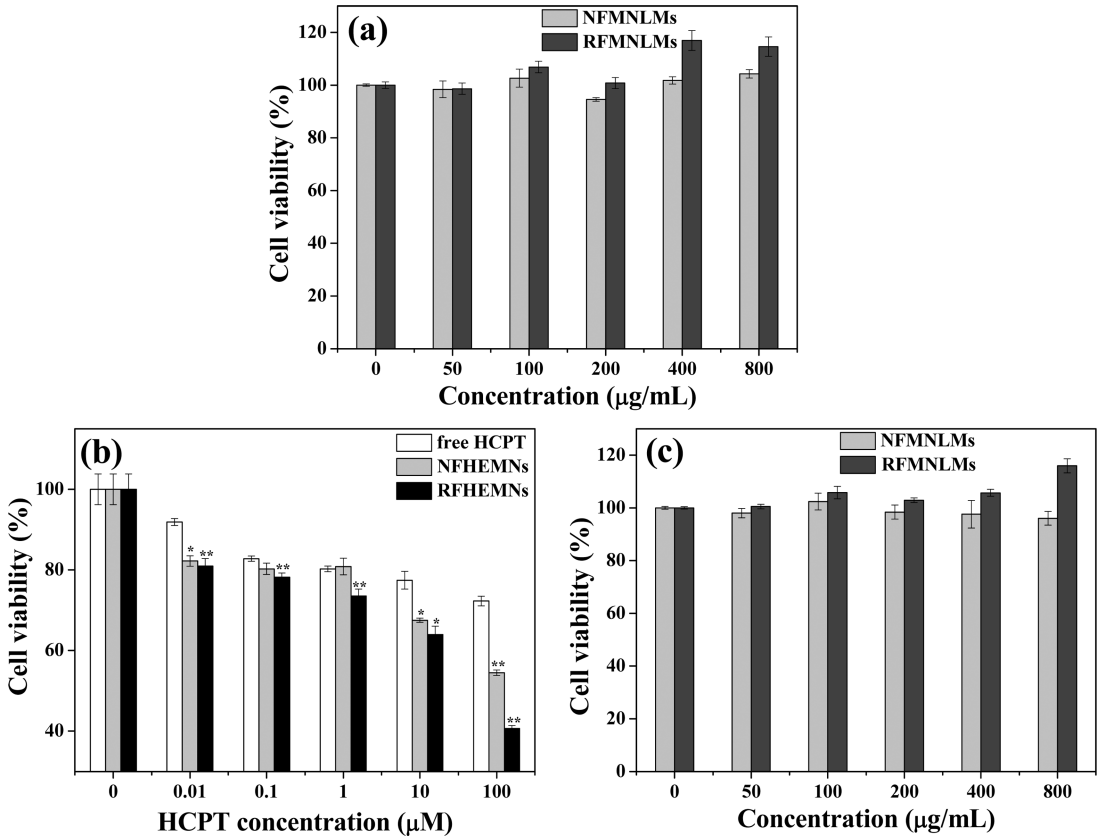

Figure 5. In vitro cell viability of (a) HEK293T and (c) A549 cells after incubation with the NFMNLMs and RFMNLMs at different concentrations for 24 h. (b) Growth inhibition assay for A549 cells treated with free HCPT, NFHEMNs, and RFHEMNs at different HCPT concentrations after 24 h incubation. *P < 0.05 and **P < 0.01, NFHEMNs, and RFHEMNs relative to free HCPT. The data represent the mean ± SD from three replicates for each run.

values. The higher pH value could transform HCPT (lactone form) into the highly water-soluble carboxylate form, thus dramatically improves its solubility, which is favorable for penetrating through micelle cores and the faster release. This pH-dependent release behavior of HCPT was also reported by other groups.[43,44] The acidic intracellular environment of most cancer cells will facilitate the sustained and slow release of HCPT from RFHEMNs.

3.4. Targeted Anticancer Action of RFHEMNs in Vitro. To evaluate the targeting ability of RFHEMNs to cancer, two cell lines—A549 (human nonsmall cell lung carcinoma cells) and HEK293T (human embryonic kidney cells 293T) cells were chosen for in vitro cell viability study. It has been documented that A549 cells can overexpress the integrin $\alpha_V\beta_3$, whereas the HEK293T cells express almost no $\alpha_V\beta_3$.[45,46]

As a drug delivery carrier, the biocompatibility/safety issue is the first priority that need to be considered. Therefore, the nonfunctionalized and RGDC-functionalized, magnetite nanoparticles-loaded micelles (denoted as NFMNLMs and RFMNLMs respectively) without HCPT loading were prepared and their cytotoxicity was determined in normal HEK293T cells. It can be seen from Figure 5a that NFMNLMs and RFMNLMs exhibited no clear cytotoxicity against HEK293T cells in a broad concentration range (50−800 μg/mL) for 24 h, the cell viability remained above 94% and even exceeded 100% at concentrations of 100, 400, and 800 μg/mL. That is, NFMNLMs and RFMNLMs without HCPT loading have an excellent biocompatibility and can serve as a well-designed drug delivery system.

Then to examine the targeting efficiency and pharmacological activity of RFHEMNs, the inhibitory effect of free HCPT, NFHEMNs and RFHEMNs on A549 cells was tested (Figure 5b). A dose-dependent cytotoxity to A549 cells was observed for free HCPT, NFHEMNs and RFHEMNs. Moreover, it is very interesting to note that a much stronger suppression effect on A549 cell growth and proliferation was observed for RFHEMNs than that of free HCPT and NFHEMNs at each concentration. In RFHEMNs, the RGDC tetrapeptide was conjugated to act as a targeting ligand. The strong binding affinity between $\alpha_V\beta_3$ and RGD-containing peptides facilitates the intracellular uptake of RFHEMNs through integrin meditated endocytosis, which accounted for the enhanced antitumor potency. In addition, we also found that NFHEMNs and RFHEMNs were superior to free HCPT whether with RGDC coupling or not, indicating that the therapeutic effect of HCPT was significantly improved when incorporated into magnetic nanohybrids. Cytotoxicity of NFMNLMs and RFMNLMs against A549 cells was also determined, and the results in Figure 5c suggested that almost no cytotoxicity was detected at all the tested concentrations, so the antitumor activity of NFHEMNs and RFHEMNs was ascribed to HCPT.

3.5. Cell Cycle Arrest Induced by RFHEMNs. Typically, the progression of cell cycle in eukaryotes is a complex process including the resting G0 phase, and cell growth involving G1, S and G2/M phases in a stepwise manner. The antitumor mechanism of camptothecin (CPT) and its derivatives such as HCPT is based on inhibition of DNA replication and RNA

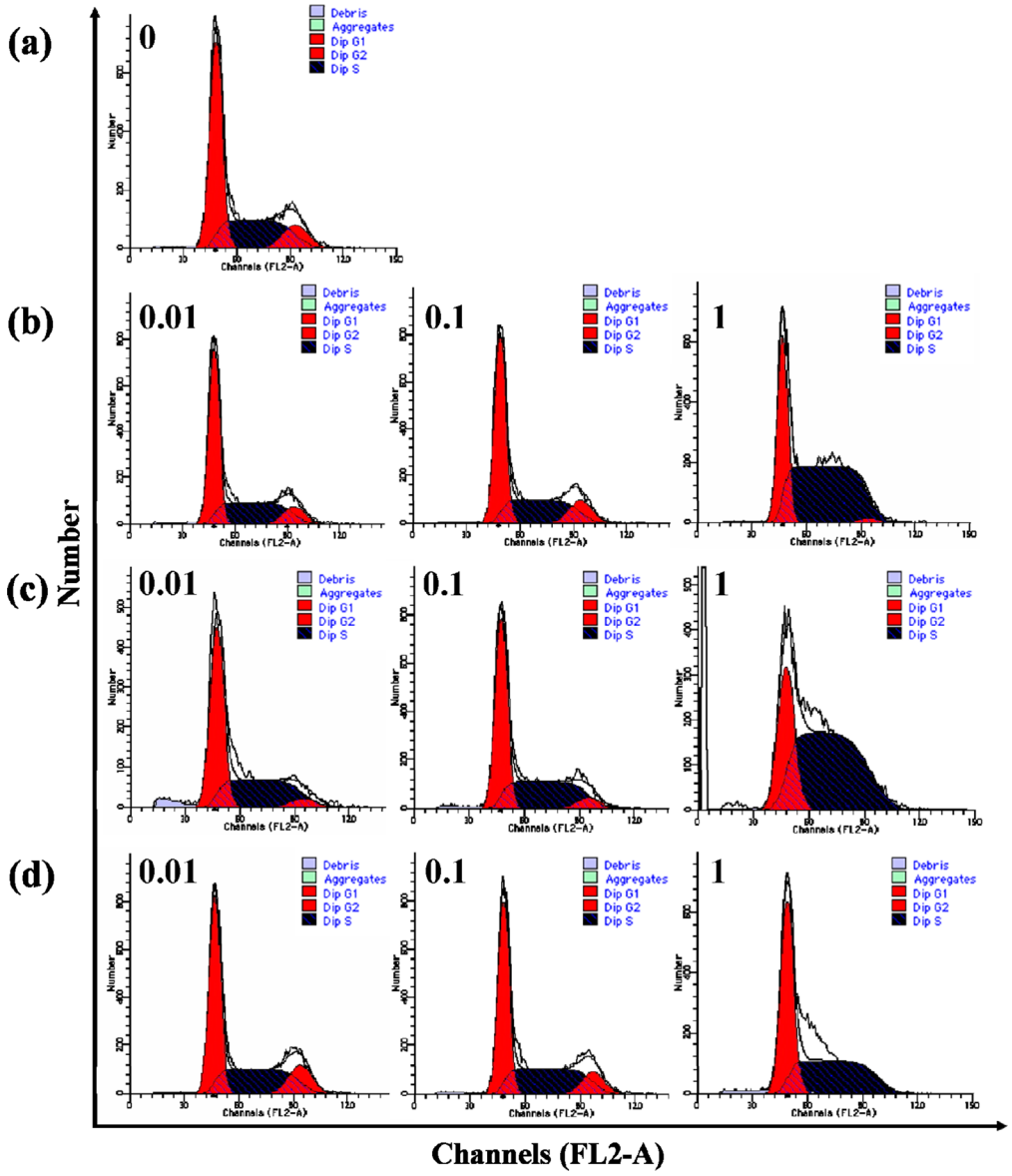

Figure 6. Cell cycle distribution of A549 cells after treatment with (a) control medium, (b) free HCPT, (c) NFHEMNs, and (d) RFHEMNs (with HCPT concentrations of 0.01, 0.1, and 1 μM) for 12 h and analyzed by flow cytometry.

transcription by stabilizing the cleavable complexes formed between nuclear enzyme topoisomerase I (topo I) and DNA.[21,28,44] It has been reported that HCPT is a cell cycle-specific agent that mainly arrests cells during DNA synthesis (S phase) and suppresses the growth and proliferation of cells.[47]

To test whether the three HCPT formulations could affect the cell cycle progression, A549 cells were exposed to free HCPT, NFHEMNs and RFHEMNs with different HCPT concentration for 12 h and then were subjected to flow cytometric analysis after DNA staining. As shown in Figure 6 and Table 2, exposure of A549 cells to three HCPT formulations resulted in a significant S phase arrest, and the proportion of cells in the S phase of the cell cycle increased in a concentration-dependent manner during the tested range of concentration. These results revealed that introduction of the three HCPT formulations leaded to a redistribution of the cell cycle phase, which might remarkably influence the proliferation of A549 cells. Furthermore, RFHEMNs did not exert the strongest effect of S phase arrest even though the highest cytotoxicity to A549 cells was observed, indicating that the cytotoxicity of HCPT is associated not only with the alteration of cell cycle and DNA fragmentation but also with the triggering of apoptosis. Actually, the apoptosis-induction activity of HCPT has been reported in our previous study.[22]

3.6. Enhanced Anti-Cell-Migration Activity of RFHEMNs. Having shown the potent in vitro antitumor and cell cycle arrest effects of RFHEMNs, their inhibitory action on cell migration was tentatively investigated. First of all, wound closure experiments were conducted to examine the effect of three HCPT formulations on collective cell migration. The scratched monolayer was photographed at 0 and 24 h (Figure 7a), it is easy to find that the wound closure was obviously inhibited by three HCPT formulations compare to the control group, the inhibition rate was in a rank order of RFHEMNs > NFHEMNs > free HCPT > control. To quantify the wound healing, the scratch width was determined and the average linear speed of the wound edges was calculated. As shown in Figure 7b, cell migration speed of control group was 13.53 μm/

Table 2. Proportion of G_1, S, and G_2 Phase A549 Cells after Exposing to Three Different HCPT Formulations (with HCPT concentrations of 0.01, 0.1, and 1 μM) for 12 h[a]

	cell cycle distribution of A549 cells (%)		
HCPT concentration (μM)	G_1	S	G_2
control			
0	53.14	35.23	11.63
free HCPT			
0.01	52.21	35.28	12.51
0.1	52.36	37.17	10.48
1	32.90	65.76	1.33
NFHEMNs			
0.01	53.92	41.29	4.79
0.1	52.26	42.08	5.66
1	31.40	68.60	0
RFHEMNs			
0.01	49.73	36.15	14.12
0.1	48.98	40.01	11.01
1	51.93	48.07	0

[a]These data were obtained from Figure 6.

h. After treatment with free HCPT, NFHEMNs, and RFHEMNs (with an HCPT concentration of 100 μM) for 6 h, wound closure speed decreased to 8.62, 4.50, and 1.36 μm/h, respectively, and there are statistically significant differences ($P < 0.01$) relative to control medium. Interestingly, RFHEMNs exhibited the highest anti-cell-migration activity.

This superior anti-cell-migration activity of RFHEMNs may be explained by several factors. First, the active lactone form of HCPT in RFHEMNs or NFHEMNs is kept intact due to the protection of the polymer micelles. This can extend the drug's half-life in the medium. Moreover, receptor (integrin $\alpha_V\beta_3$)-meditated endocytosis enhanced the cellular internalization of RFHEMNs by A549 cells, thus increased the uptake of HCPT. In addition, RGDC peptide on the surface of RFHEMNs can selectively bind with integrin $\alpha_V\beta_3$ and affect its functions which in turn inhibits cell migration. It is known that integrins including $\alpha_V\beta_3$ are crucial for the attachment of cells to extracellular matrix during the process of cell invasion and migration.[33]

Then, a filter membrane migration assay was performed to determine whether RFHEMNs influence single cell migration. In this assay, A549 cells were seeded on the top side of the membrane and were allowed to migrate through the pores of the membrane into the lower compartment, in which chemotactic factor (DMEM medium containing 10% FBS) is present. It can be seen from Figure 8a that about 59.27% A549 cells migrate across the pored filter membrane to the lower side of the filter membrane during 24 h incubation. Yet, the migration rate of A549 cells decreased dramatically when exposed to free HCPT, NFHEMNs and RFHEMNs (with an HCPT concentration of 100 μM) for 6 h, with a migration rate of 42.14%, 38.66% and 27.34% respectively, and there are statistically significant differences ($P < 0.01$) as compared to the control cells. Accordingly, the inhibition rate of migration was calculated, and the results are presented in Figure 8b. These results are in accordance with those obtained from wound healing assays and suggest that RFHEMNs exerted the strongest suppress effect on cell migration with an inhibition rate of 53.87%, nearly twice that free HCPT (28.90%). The inhibitory action on cell migration was also in an order of RFHEMNs > NFHEMNs > free HCPT > control. Together, these results indicate that RFHEMNs displayed an inspiring inhibitory effect on migration of A549 cells and may be a promising candidate for chemotherapy of metastatic cancer. Further studies are required to elucidate the underlying mechanisms for this enhanced anti-cell-migration activity of RFHEMNs.

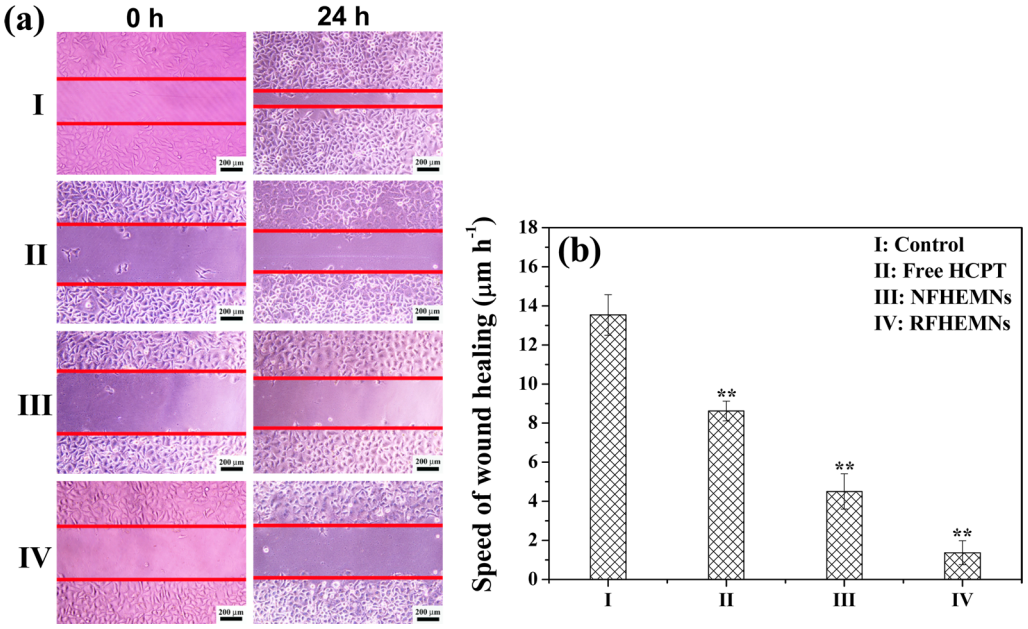

Figure 7. Wound-healing assays for determining cell migration. (a) Scratch width of control and treated A549 cells at 0 and 24 h. Cells were treated with control medium (I), free HCPT (II), NFHEMNs (III), and RFHEMNs (IV) (with an HCPT concentration of 100 μM) for 6 h. Wound edges are marked with red lines. (b) Quantified speed of wound healing ($n = 3$, mean ± SD, ** denote $P < 0.01$ versus control cells).

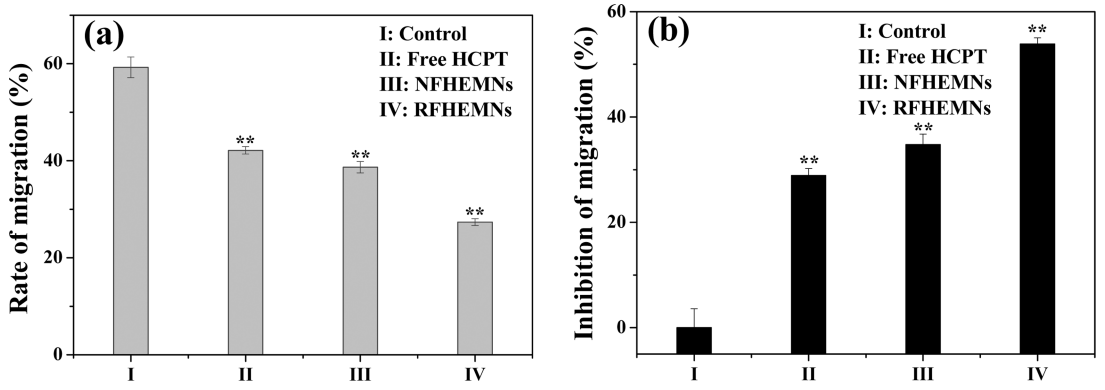

Figure 8. Transwell analysis of cell migration. (a) Migration rate and (b) inhibition of migration of control and treated A549 cells. Cells were exposed to control medium (I), free HCPT (II), NFHEMNs (III), and RFHEMNs (IV) (with an HCPT concentration of 100 μM) for 6 h. Data in the figures are presented as mean ± SD of three independent experiments. $^{**}P < 0.01$, relative to control cells.

4. CONCLUSION

In summary, RGDC functionalized and 10-hydroxycamptothecin-encapsulated magnetic nanohybrids (RFHEMNs) were successfully fabricated and carefully characterized in this study. The RFHEMNs have a well-defined spherical shape, a size around 50 nm and good superparamagnetism. We demonstrated that RFHEMNs exhibits significantly higher in vitro antitumor potency against A549 cells, in comparison to the free drug HCPT and nontargeting NFHEMNs. Flow cytometry analysis indicated that this antiproliferative efficacy was possibly mediated by an arrest of S-phase of the cell cycle. It is inspiring to note that RFHEMNs display much stronger anti-cell-migration activity than free HCPT and NFHEMNs as determined by in vitro wound-healing assay and transwell assay. Therefore, our results suggested that the RFHEMNs hold great potential to be a powerful nanoscale drug delivery system for targeted chemotherapy of integrin $\alpha_V\beta_3$-overexpressing metastatic tumors.

■ ASSOCIATED CONTENT

Supporting Information

SEM image of RFHEMNs. This material is available free of charge via the Internet at http://pubs.acs.org.

■ AUTHOR INFORMATION

Corresponding Authors

*Tel.: +86-431-85155226. Fax: +86-431-85155226. E-mail: xuli@jlu.edu.cn.

*E-mail: guoyi@jlu.edu.cn.

Notes

The authors declare no competing financial interest.

■ ACKNOWLEDGMENTS

The work was supported by the National Natural Science Foundation of China (81271697), the Specialized Research Fund for the Doctoral Program of Higher Education of China (20120061110021), and the Social Development Project of Science and Technology Department of Jilin Province, China (20106031, 20120967, YYZX201264, 20130206069GX), the Fundamental Research Funds for the Central Universities, "Significant New Drug Creation" Science and Technology Major Program (No.2012ZX09503001-003), and the Science Foundation for Youths of Shanxi Province (2013021014-1).

■ REFERENCES

(1) Nishiyama, N.; Kataoka, K. Current State, Achievements, and Future Prospects of Polymeric Micelles as Nanocarriers for Drug and Gene Delivery. *Pharmacol. Ther.* **2006**, *112*, 630−648.

(2) Torchilin, V. P. Micellar Nanocarriers: Pharmaceutical Perspectives. *Pharm. Res.* **2007**, *24*, 1−16.

(3) Talelli, M.; Rijcken, C. J.; Hennink, W. E.; Lammers, T. Polymeric Micelles for Cancer Therapy: 3 C's to Enhance Efficacy. *Curr. Opin. Solid State Mater. Sci.* **2012**, *16*, 302−309.

(4) Xiong, X. B.; Binkhathlan, Z.; Molavi, O.; Lavasanifar, A. Amphiphilic Block Co-Polymers: Preparation and Application in Nanodrug and Gene Delivery. *Acta Biomater.* **2012**, *8*, 2017−2033.

(5) Zhang, X.; Huang, Y.; Li, S. Nanomicellar Carriers for Targeted Delivery of Anticancer Agents. *Ther. Delivery* **2014**, *5*, 53−68.

(6) Sutton, D.; Nasongkla, N.; Blanco, E.; Gao, J. Functionalized Micellar Systems for Cancer Targeted Drug Delivery. *Pharm. Res.* **2007**, *24*, 1029−1046.

(7) Ding, J.; Chen, J.; Li, D.; Xiao, C.; Zhang, J.; He, C.; Zhuang, X.; Chen, X. Biocompatible Reduction-Responsive Polypeptide Micelles as Nanocarriers for Enhanced Chemotherapy Efficacy In Vitro. *J. Mater. Chem. B* **2013**, *1*, 69−81.

(8) Lv, Y.; Ding, G.; Zhai, J.; Guo, Y.; Nie, G.; Xu, L. A Superparamagnetic Fe_3O_4-Loaded Polymeric Nanocarrier for Targeted Delivery of Evodiamine with Enhanced Antitumor Efficacy. *Colloids Surf., B* **2013**, *110*, 411−418.

(9) Reddy, L. H.; Arias, J. L.; Nicolas, J.; Couvreur, P. Magnetic Nanoparticles: Design and Characterization, Toxicity and Biocompatibility, Pharmaceutical and Biomedical Applications. *Chem. Rev.* **2012**, *112*, 5818−5878.

(10) Ling, D.; Hyeon, T. Chemical Design of Biocompatible Iron Oxide Nanoparticles for Medical Applications. *Small* **2013**, *9*, 1450−1466.

(11) Liu, Z.; Li, M.; Li, Z.; Pu, F.; Ren, J.; Qu, X. Easy Access to Selective Binding and Recyclable Separation of Histidine-Tagged Proteins Using Ni^{2+}-Decorated Superparamagnetic Nanoparticles. *Nano Res.* **2012**, *5*, 450−459.

(12) Zhang, Y.; Yang, Y.; Ma, W.; Guo, J.; Lin, Y.; Wang, C. Uniform Magnetic Core/Shell Microspheres Functionalized with Ni^{2+}−Iminodiacetic Acid for One Step Purification and Immobilization of His-Tagged Enzymes. *ACS Appl. Mater. Interfaces* **2013**, *5*, 2626−2633.

(13) Liu, F.; Jin, Y.; Liao, H.; Cai, L.; Tong, M.; Hou, Y. Facile Self-Assembly Synthesis of Titanate/Fe_3O_4 Nanocomposites for the Efficient Removal of Pb^{2+} from Aqueous Systems. *J. Mater. Chem. A* **2013**, *1*, 805−813.

(14) Liang, M.; Fan, K.; Pan, Y.; Jiang, H.; Wang, F.; Yang, D.; Lu, D.; Feng, J.; Zhao, J.; Yang, L.; Yan, X. Fe_3O_4 Magnetic Nanoparticle Peroxidase Mimetic-Based Colorimetric Assay for the Rapid Detection of Organophosphorus Pesticide and Nerve Agent. *Anal. Chem.* **2013**, *85*, 308−312.

(15) Mok, H.; Zhang, M. Superparamagnetic Iron Oxide Nanoparticle-Based Delivery Systems for Biotherapeutics. *Expert Opin. Drug Delivery* **2013**, *10*, 73−87.
(16) Lee, N.; Hyeon, T. Designed Synthesis of Uniformly Sized Iron Oxide Nanoparticles for Efficient Magnetic Resonance Imaging Contrast Agents. *Chem. Soc. Rev.* **2012**, *41*, 2575−2589.
(17) Li, K.; Ding, D.; Huo, D.; Pu, K. Y.; Thao, N. N. P.; Hu, Y.; Li, Z.; Liu, B. Conjugated Polymer Based Nanoparticles as Dual-Modal Probes for Targeted In Vivo Fluorescence and Magnetic Resonance Imaging. *Adv. Funct. Mater.* **2012**, *22*, 3107−3115.
(18) Sahoo, B.; Devi, K. S.; Banerjee, R.; Maiti, T. K.; Pramanik, P.; Dhara, D. Thermal and pH Responsive Polymer-Tethered Multifunctional Magnetic Nanoparticles for Targeted Delivery of Anticancer Drug. *ACS Appl. Mater. Interfaces* **2013**, *5*, 3884−3893.
(19) Yang, Y.; Zhang, X.; Yu, C.; Hao, X.; Jie, J.; Zhou, M.; Zhang, X. Smart Nanorods for Highly Effective Cancer Theranostic Applications. *Adv. Healthcare Mater.* **2014**, *3*, 906−915.
(20) Zhu, H.; Cao, J.; Cui, S.; Qian, Z.; Gu, Y. Enhanced Tumor Targeting and Antitumor Efficacy via Hydroxycamptothecin-Encapsulated Folate-Modified N-Succinyl-N′-Octyl Chitosan Micelles. *J. Pharm. Sci.* **2013**, *102*, 1318−1332.
(21) Li, Q.; Liu, C.; Zhao, X.; Zu, Y.; Wang, Y.; Zhang, B.; Zhao, D.; Zhao, Q.; Su, L.; Gao, Y.; Sun, B. Preparation, Characterization and Targeting of Micronized 10-Hydroxycamptothecin-Loaded Folate-Conjugated Human Serum Albumin Nanoparticles to Cancer Cells. *Int. J. Nanomed.* **2011**, *6*, 397−405.
(22) Ding, G. B.; Liu, H. Y.; Lv, Y. Y.; Liu, X. F.; Guo, Y.; Sun, C. K.; Xu, L. Enhanced In Vitro Antitumor Efficacy and Strong Anti-Cell-Migration Activity of a Hydroxycamptothecin-Encapsulated Magnetic Nanovehicle. *Chem.—Eur. J.* **2012**, *18*, 14037−14046.
(23) Hong, M.; Zhu, S.; Jiang, Y.; Tang, G.; Sun, C.; Fang, C.; Shi, B.; Pei, Y. Novel Anti-tumor Strategy: PEG-Hydroxycamptothecin Conjugate Loaded Transferrin-PEG- Nanoparticles. *J. Controlled Release* **2010**, *141*, 22−29.
(24) Ding, G. B.; Liu, H. Y.; Wang, Y.; Lu, Y. Y.; Wu, Y.; Guo, Y.; Xu, L. Fabrication of a Magnetite Nanoparticle-loaded Polymeric Nanoplatform for Magnetically Guided Drug Delivery. *Chem. Res. Chin. Univ.* **2013**, *29*, 103−109.
(25) Ci, T. Y.; Chen, L.; Li, T.; Chang, G. T.; Yu, L.; Ding, J. D. Effects of Amphiphilic Block Copolymers on the Equilibrium Lactone Fractions of Camptothecin Analogues at Different pHs. *Biomater. Sci.* **2013**, *1*, 1235−1243.
(26) Gan, L.; Gao, Y. P.; Zhu, C. L.; Zhang, X. X.; Gan, Y. Novel pH-Sensitive Lipid−Polymer Composite Microspheres of 10-Hydroxycamptothecin Exhibiting Colon-Specific Biodistribution and Reduced Systemic Absorption. *J. Pharm. Sci.* **2013**, *102*, 1752−1759.
(27) Kong, X.; Yu, K.; Yu, M.; Feng, Y.; Wang, J.; Li, M.; Chen, Z.; He, M.; Guo, R.; Tian, R.; Li, Y.; Wu, W.; Hong, Z. A Novel Multifunctional Poly(amidoamine) Dendrimeric Delivery System with Superior Encapsulation Capacity for Targeted Delivery of the Chemotherapy Drug 10-Hydroxycamptothecin. *Int. J. Pharm.* **2014**, *465*, 378−387.
(28) Zhang, G.; Ding, L.; Renegar, R.; Wang, X.; Lu, Q.; Huo, S.; Chen, Y. H. Hydroxycamptothecin-Loaded Fe_3O_4 Nanoparticles Induce Human Lung Cancer Cell Apoptosis through Caspase-8 Pathway Activation and Disrupt Tight Junctions. *Cancer Sci.* **2011**, *102*, 1216−1222.
(29) Qu, J. B.; Shao, H. H.; Jing, G. L.; Huang, F. PEG-Chitosan-Coated Iron Oxide Nanoparticles with High Saturated Magnetization as Carriers of 10-Hydroxycamptothecin: Preparation, Characterization and Cytotoxicity Studies. *Colloids Surf., B* **2013**, *102*, 37−44.
(30) Khandare, J.; Calderon, M.; Dagia, N. M.; Haag, R. Multifunctional Dendritic Polymers in Nanomedicine: Opportunities and Challenges. *Chem. Soc. Rev.* **2012**, *41*, 2824−2848.
(31) Chaffer, C. L.; Weinberg, R. A. A Perspective on Cancer Cell Metastasis. *Science* **2011**, *331*, 1559−1564.
(32) Yamaguchi, H.; Wyckoff, J.; Condeelis, J. Cell migration in tumors. *Curr. Opin. Cell Biol.* **2005**, *17*, 559−564.
(33) Hood, J. D.; Cheresh, D. A. Role of Integrins in Cell Invasion and Migration. *Nat. Rev. Cancer* **2002**, *2*, 91−100.
(34) Fang, J.; Nakamura, H.; Maeda, H. The EPR Effect: Unique Features of Tumor Blood Vessels for Drug Delivery, Factors Involved, and Limitations and Augmentation of the Effect. *Adv. Drug Delivery Rev.* **2011**, *63*, 136−151.
(35) Cabral, H.; Matsumoto, Y.; Mizuno, K.; Chen, Q.; Murakami, M.; Kimura, M.; Terada, Y.; Kano, M. R.; Miyazono, K.; Uesaka, M.; Nishiyama, N.; Kataoka, K. Accumulation of Sub-100 nm Polymeric Micelles in Poorly Permeable Tumours Depends on Size. *Nat. Nanotechnol.* **2011**, *6*, 815−823.
(36) Wiradharma, N.; Zhang, Y.; Venkataraman, S.; Hedrick, J. L.; Yang, Y. Y. Self-Assembled Polymer Nanostructures for Delivery of Anticancer Therapeutics. *Nano Today* **2009**, *4*, 302−317.
(37) Chen, K.; Chen, X. Integrin Targeted Delivery of Chemotherapeutics. *Theranostics* **2011**, *1*, 189−200.
(38) Ye, Y.; Chen, X. Integrin Targeting for Tumor Optical Imaging. *Theranostics* **2011**, *1*, 102−126.
(39) Ding, G.; Guo, Y.; Lv, Y.; Liu, X.; Xu, L.; Zhang, X. A Double-Targeted Magnetic Nanocarrier with Potential Application in Hydrophobic Drug Delivery. *Colloids Surf., B* **2012**, *91*, 68−76.
(40) Zhang, Z.; Ni, J.; Chen, L.; Yu, L.; Xu, J. W.; Ding, J. D. Biodegradable and Thermoreversible PCLA−PEG−PCLA Hydrogel as a Barrier for Prevention of Post-Operative Adhesion. *Biomaterials* **2011**, *32*, 4725−4736.
(41) Devadasu, V. R.; Bhardwaj, V.; Kumar, M. N. V. R. Can Controversial Nanotechnology Promise Drug Delivery? *Chem. Rev.* **2013**, *113*, 1686−1735.
(42) Huang, X. G.; Jiang, X. L.; Yang, Q. Z.; Chu, Y. F.; Zhang, G. Y.; Yang, Y.; Zhuo, R. X. Triple-Stimuli (pH/Thermo/Reduction) Sensitive Copolymers for Intracellular Drug Delivery. *J. Mater. Chem. B* **2013**, *1*, 1860−1868.
(43) Zhang, L.; Yang, M.; Wang, Q.; Li, Y.; Guo, R.; Jiang, X.; Yang, C.; Liu, B. 10-Hydroxycamptothecin Loaded Nanoparticles: Preparation and Antitumor Activity in Mice. *J. Controlled Release* **2007**, *119*, 153−162.
(44) Guo, X. M.; Guo, B.; Zhang, Q.; Sun, X. Absorption of 10-Hydroxycamptothecin on Fe_3O_4 Magnetite Nanoparticles with Layer-by-Layer Self-assembly and Drug Release Response. *Dalton Trans.* **2011**, *40*, 3039−3046.
(45) Ye, Y.; Xu, B.; Nikiforovich, G. V.; Bloch, S.; Achilefu, S. Exploring New Near-Infrared Fluorescent Disulfide-Based Cyclic RGD Peptide Analogs for Potential Integrin-Targeted Optical Imaging. *Bioorg. Med. Chem. Lett.* **2011**, *21*, 2116−2120.
(46) Oba, M.; Fukushima, S.; Kanayama, N.; Aoyagi, K.; Nishiyama, N.; Koyama, H.; Kataoka, K. Cyclic RGD Peptide-Conjugated Polyplex Micelles as a Targetable Gene Delivery System Directed to Cells Possessing $\alpha_V\beta_3$ and $\alpha_V\beta_5$ Integrins. *Bioconjugate Chem.* **2007**, *18*, 1415−1423.
(47) Yin, X.; Sun, H.; Yu, D.; Liang, Y.; Yuan, Z.; Ge, Y. Hydroxycamptothecin Induces Apoptosis of Human Tenon's Capsule Fibroblasts by Activating the PERK Signaling Pathway. *Invest. Ophthalmol. Visual Sci.* **2013**, *54*, 4749−4758.